nanomaterials

MDPI

Article

Highly Stable and Enhanced Performance of p–i–n Perovskite Solar Cells via Cuprous Oxide Hole-Transport Layers

Tung-Han Chuang [1], Yin-Hung Chen [1], Shikha Sakalley [2,3], Wei-Chun Cheng [2], Choon Kit Chan [4], Chih-Ping Chen [3,*] and Sheng-Chi Chen [3,5,*]

[1] Institute of Materials Science and Engineering, National Taiwan University, Taipei 106, Taiwan
[2] Department of Mechanical Engineering, National Taiwan University of Science and Technology, Taipei 106, Taiwan
[3] Department of Materials Engineering and Center for Plasma and Thin Film Technologies, Ming Chi University of Technology, New Taipei City 243, Taiwan
[4] Mechanical Engineering Department, Faculty of Engineering and Quantity Surveying, INTI International University, Nilai 71800, Negeri Sembilan, Malaysia
[5] College of Engineering and Center for Green Technology, Chang Gung University, Taoyuan 333, Taiwan
* Correspondence: cpchen@mail.mcut.edu.tw (C.-P.C.); chensc@mail.mcut.edu.tw (S.-C.C.)

Abstract: Solar light is a renewable source of energy that can be used and transformed into electricity using clean energy technology. In this study, we used direct current magnetron sputtering (DCMS) to sputter p-type cuprous oxide (Cu_2O) films with different oxygen flow rates (f_{O2}) as hole-transport layers (HTLs) for perovskite solar cells (PSCs). The PSC device with the structure of ITO/Cu_2O/perovskite/[6,6]-phenyl-C_{61}-butyric acid methyl ester ($PC_{61}BM$)/bathocuproine (BCP)/Ag showed a power conversion efficiency (PCE) of 7.91%. Subsequently, a high-power impulse magnetron sputtering (HiPIMS) Cu_2O film was embedded and promoted the device performance to 10.29%. As HiPIMS has a high ionization rate, it can create higher density films with low surface roughness, which passivates surface/interface defects and reduces the leakage current of PSCs. We further applied the superimposed high-power impulse magnetron sputtering (superimposed HiPIMS) derived Cu_2O as the HTL, and we observed PCEs of 15.20% under one sun (AM1.5G, 1000 Wm^{-2}) and 25.09% under indoor illumination (TL-84, 1000 lux). In addition, this PSC device outperformed by demonstrating remarkable long-term stability via retaining 97.6% (dark, Ar) of its performance for over 2000 h.

Keywords: Cu_2O films; solar cell; DCMS; HiPIMS; superimposed HiPIMS; hole-transport layer (HTL); power conversion efficiency (PCE)

check for updates

Citation: Chuang, T.-H.; Chen, Y.-H.; Sakalley, S.; Cheng, W.-C.; Chan, C.K.; Chen, C.-P.; Chen, S.-C. Highly Stable and Enhanced Performance of p–i–n Perovskite Solar Cells via Cuprous Oxide Hole-Transport Layers. *Nanomaterials* **2023**, *13*, 1363. https://doi.org/10.3390/nano13081363

Academic Editor: Elias Stathatos

Received: 6 March 2023
Revised: 6 April 2023
Accepted: 10 April 2023
Published: 14 April 2023

Copyright: © 2023 by the authors. Licensee MDPI, Basel, Switzerland. This article is an open access article distributed under the terms and conditions of the Creative Commons Attribution (CC BY) license (https://creativecommons.org/licenses/by/4.0/).

1. Introduction

Solar energy is the most abundant and promising alternative to fossil energy. It can be collected and converted easily in the form of electricity for industrial and household usage via various technologies such as silicon-based solar cells (SSCs) [1], dye-sensitized solar cells (DSSCs) [2], organic photovoltaics (OPVs) [3,4], and perovskite solar cells (PSCs) [5,6]. Among these, PSCs have gained the most interest due to their impressive power conversion efficiency (PCE) [7–10]. The first PSC, introduced by Miyasaka in 2009, had a PCE of 3.8% [11], which now exceeds 25.7% [12] within quite a few years of development. Because of their easy fabrication in low temperatures, inexpensive solution process, and excellent performance attributed to outstanding optoelectronic properties [13–25], PSCs have attracted more attention. Perovskites typically have the chemical formula ABX_3, where A is a monovalent cation (such as methyl ammonium [$CH_3NH_3^+$ (MA)], NH = $CHNH_3^+$ (FA), or Cs^+), B is either a Pb^{2+} or Sn^{2+} divalent metallic cation, and X is a halide anion (I^-, Br^-, or Cl^-) [26,27].

The classifications of PSC device architecture based on arrangement of heterojunctions are n−i−p (conventional) and p−i−n (inverted). The selection of materials for hole-transport layers (HTLs) shows the impact on the performance and stability of PSCs. Commonly used hole-transport materials (HTMs) are 2,2′,7,7′-tetrakis-(N, N-di-4-methoxyphenylamino)-9,9′-spirobifluorene (Spiro-OMeTAD) [28], poly(3,4-ethylene dioxythiophene) (PEDOT:PSS) [29], poly(3-hexylthiophene) (P3HT) [30], and poly[bis(4-phenyl) (2,4,6-trimethylphenyl)-amine] (PTAA) [31]. These organic materials become highly unstable when exposed to air (moisture) for a long time. Thereby, the replacement of organic HTMs with inorganic HTMs is being considered for comparatively higher stability. For instance, NiO_x has been used as an efficient HTL possessing an outstanding performance with excellent air stability [19,32,33]. Cuprous oxide (Cu_2O) offers a band gap in the range of 2.2–2.8 eV with an enormous hole mobility of (100 $cm^2V^{-1}s^{-1}$) [34–36] and the features of nontoxicity, abundance on the earth's crust, and low manufacturing cost, which make it a candidate for HTLs of PSCs [37]. Relentless research on Cu_2O-based, transparent thin-film PSCs has achieved significant theoretical energy conversion efficiency [38,39]. There are various chemical/solution and physical deposition methods to prepare Cu_2O thin films, such as sol-gel [40], thermal oxidation [34], chemical vapor deposition [41], RF/DC sputtering [42,43], electrodeposition [44], pulsed laser deposition [45], and high-power impulse magnetron sputtering (HiPIMS) [46]. Even though Cu_2O thin films have outstanding properties, it is still challenging to deposit uniform, dense, smooth, and pinhole-free layers for PSC application.

Various sputtering methods have been considered, such as direct current magnetron sputtering (DCMS) (i.e, a plasma process used for film deposition). The HiPIMS technique offers a high ionization rate of sputtered target atoms and high plasma density, which is advantageous for metal-oxide thin-film deposition [47]. Unfortunately, HiPIMS has the drawback of a low deposition rate, which limits its application. Here, middle-frequency (MF) pulses during the off-time of HiPIMS, also known as superimposed HiPIMS (HiPIMS+MF), step in to overcome the deposition rate of the HiPIMS process without sacrificing the target ionization rate [48]. In this work, we demonstrated Cu_2O as the HTLs of PSCs from different sputtering modes (DCMS, HiPIMS, and superimposed HiPIMS). We analyzed the structural, morphological, and optoelectronic properties of Cu_2O derived PSCs. The DC, HiPIMS, and superimposed HiPIMS derived devices showed performances of 7.12 ± 0.64, 9.42 ± 0.92%, and 13.04 ± 1.61%, respectively. To the best of our knowledge, the PCE of the superimposed HiPIMS derived PSCs is among the best reported for $CH_3NH_3PbI_3$ ($MAPbI_3$) based devices. Furthermore, the respective device showed remarkable stability by retaining 97.6% of its performance (i.e., storage in the dark [Ar] for over 2000 h). Hence, this study explains the effect of depositing TCO films using different sputtering modes on the PCEs and stability of PSC devices.

2. Materials and Methods

Cu_2O films (10 nm) were deposited by DCMS, HiPIMS [49], and superimposed HiPIMS [48] techniques, subsequently, on an ITO substrate. Before spin-coating the perovskite precursor solution, we used plasma to modify the Cu_2O surface for 30 s and coat the precursor solution smoothly. Details of the device fabrication and characterization of the materials are shown in the Supplementary Materials.

3. Results

We fabricated the PSCs with a p–i–n structure of Glass/ITO/Cu_2O/$MAPbI_3$/$PC_{61}BM$/BCP/Ag. Figure 1 displays the X-ray diffraction patterns of Cu_2O from DCMS and superimposed HiPIMS at different oxygen flow rates ($f_{O2} = O_2/(O_2 + Ar) \times 100\%$, Ar: Argon O_2: Oxygen). For the DCMS (Figure 1a), the increase in oxygen flow rate from f_{O2} = 10% started to form the Cu_2O phase and became pure Cu_2O phase at f_{O2} = 17.5%. Beyond this, it started to form a mixed Cu_2O phase. For the normal HiPIMS sample, we observed the Cu_2O phase at f_{O2} = 20%, which is consistent with our previously published study [49]. For the XRD

of the superimposed HiPIMS process (Figure 1b), the increase in oxygen flow rate from f_{O2} = 17.5% started to form the Cu_2O phase and became pure Cu_2O phase at f_{O2} = 30%, and later, with a further increase in f_{O2}, it became a mixed-Cu_2O phase. Accordingly, we obtained the optimal parameters for the Cu_2O phase and used them as the HTLs of PSCs for further study.

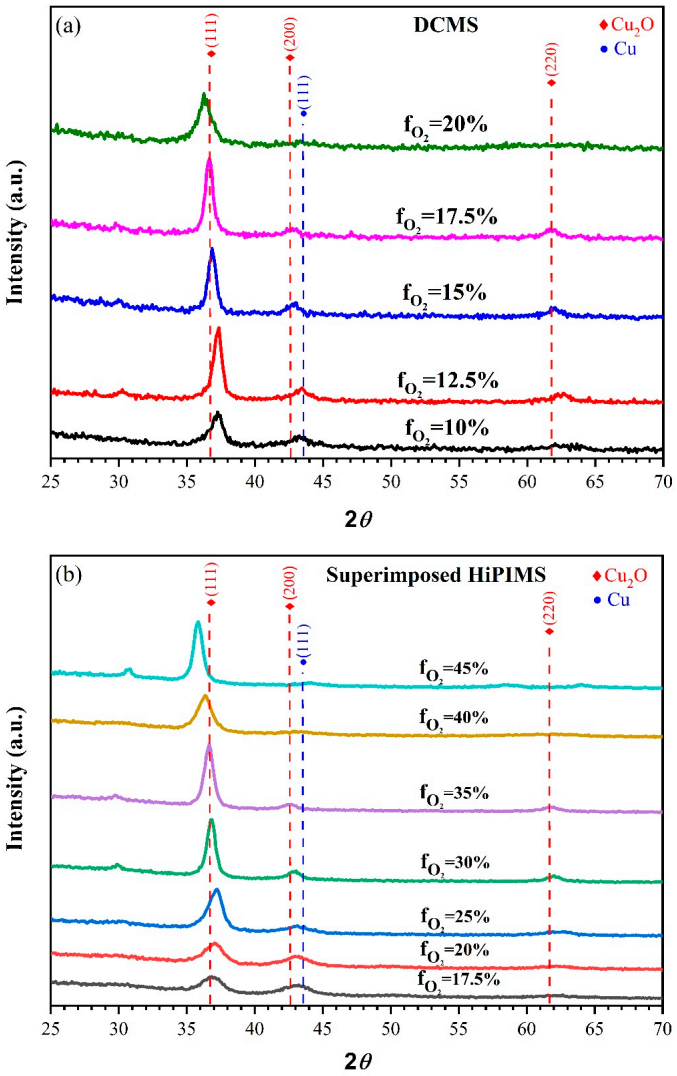

Figure 1. X-ray diffraction spectra of Cu_2O films deposited by (**a**) DCMS and (**b**) superimposed HiPIMS at different oxygen flow rates.

We determined the UV-Vis transmittance of these Cu_2O-deposited ITO samples using air as a background (Figure 2a). The transmittance of the HiPIMS sample was slightly more than 80%, while in contrast, that of the DCMS and superimposed HiPIMS samples were each a bit less than 80% (<3%), in a wavelength range (500-900 nm). Due to the high ionization rate and high-energy plasma of the HiPIMS process, it offers dense and highly crystalline Cu_2O films. Therefore, we observed higher transmittance of respective Cu_2O in comparison with the DCMS sample (i.e., the structure was less dense). Although the superimposed HiPIMS process has the same advantages as the HiPIMS process, the MF power applied during the off-time bombarded more copper that became deposited as film, possibly contributing to the decrease in transmittance.

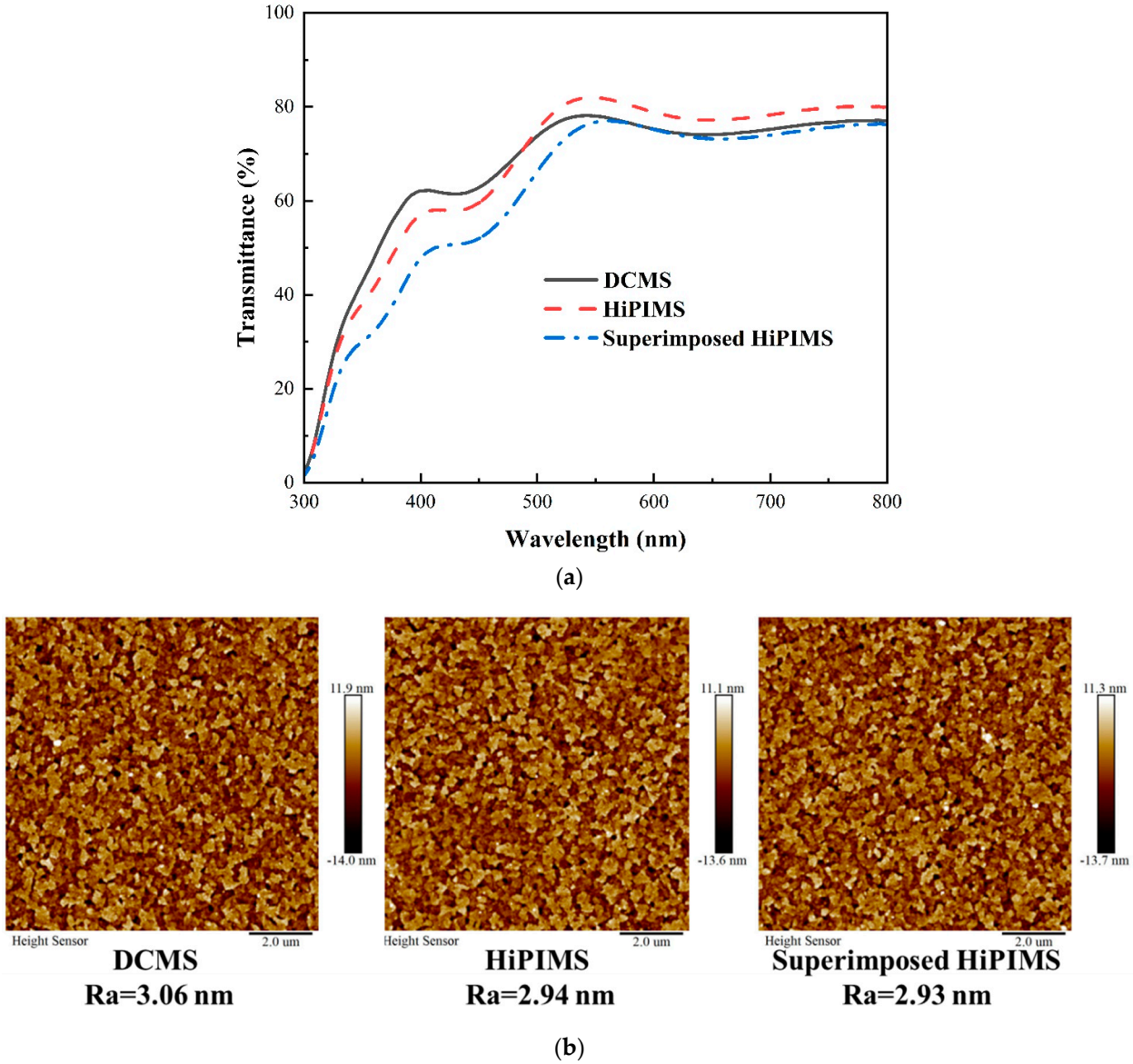

Figure 2. (**a**) UV-Vis spectra and (**b**) AFM topography images of Cu_2O films deposited using various processes.

The values of Ra (the arithmetic average of the roughness profile) of the samples were determined by tapping-mode atomic force microscopy (AFM) to understand the surface morphology of ITO/Cu_2O affecting the growth of perovskite; Figure 2b represents surface roughness through AFM images of the samples. We obtained values of Ra for the DCMS (3.06 nm), HiPIMS (2.94 nm), and superimposed HiPIMS (2.93 nm) samples. We speculated that HiPIMS would result in higher density and higher energy plasma than DCMS during deposition, which would result in a smoother surface. The superimposed HiPIMS sample had the same characteristics as the HiPIMS sample, leading to similar Ra values.

Figure 3 shows the contact angles of the ITO/Cu_2O surfaces when we dropped the perovskite precursor solution on top. As indicated in Figure 3a, the perovskite precursor formed a sphere on the HiPIMS Cu_2O samples (i.e., a high angle of 85.13°), spreading poorly on the Cu_2O surface and causing failure growth of the perovskite layer. The DCMS and superimposed HiPIMS Cu_2O samples also had high angles, of 89.95° and 69.31°, respectively, as shown in Figure S1, which also led to poor spread of the perovskite precursor. To resolve this issue, we applied a plasma treatment to induce an ultraviolet effect that modified the surface of the Cu_2O films. As indicated in Figure 3b, the Cu_2O

film became hydrophilic with a low angle of 9.99°, leading to the preferred growth of the perovskite layer.

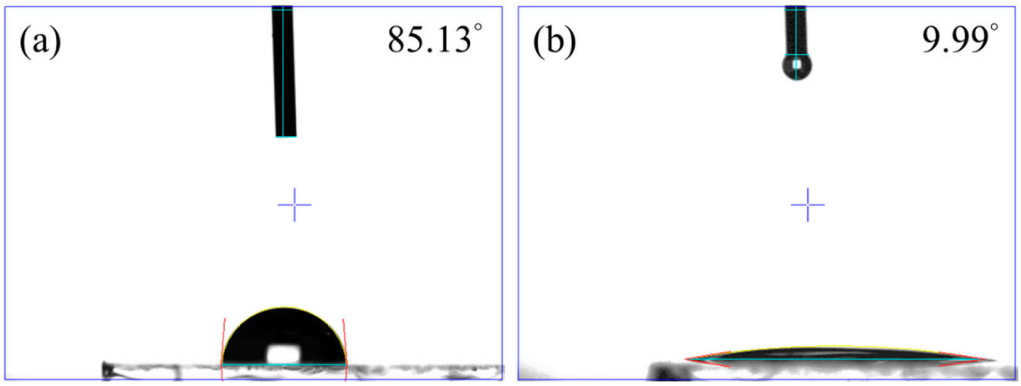

Figure 3. Cu_2O film prepared by HiPIMS (**a**) before plasma cleaning and (**b**) after plasma cleaning of the contact angle.

Table 1 and Figure 4 summarize the device performances for various Cu_2O films. Table 1 displays the standard deviations of the PSCs calculated from a minimum of three samples deposited using the same technique. The perovskite deposition was from a solution, which may cause slight variations during each deposition. Due to the variability in optoelectronic and surface properties caused by the deposition process of HTLs, the PSCs produced using various conditions of HTLs exhibited different device performances. DCMS-derived devices provided a PCE of 7.12 ± 0.64%, with a short-circuit current density (J_{sc}) of 13.74 ± 0.97 $mAcm^{-2}$, a value of open-circuit voltage (V_{oc}) of 0.89 ± 0.02 V, and a fill factor (FF) of 58.1 ± 3.93%. The HiPIMS-based devices showed slightly higher efficiency, with a PCE of 9.42 ± 0.92%, a value of J_{sc} of 17.36 ± 0.94 $mAcm^{-2}$, a value of V_{oc} of 0.90 ± 0.00 V, and an FF of 61.1 ± 6.95%. The superimposed HiPIMS devices showed the highest performance, with a PCE of 13.04 ± 1.61%, a value of J_{sc} of 19.27 ± 1.20 $mAcm^{-2}$, a value of V_{oc} of 0.98 ± 0.00 V, and an FF of 69.5 ± 4.98%. The improvement in the PCE of the overlaid HiPIMS PSCs was brought on by substantial increases in the J_{sc}, V_{oc}, and FFs. From the device's J-V curves (Figure 4), we computed the series (R_s) and shunt (R_{sh}) resistances. The resistances of the electrodes, the interfacial resistance, the hole/electron transporting layers, and the perovskite all contributed to the value of R_s. The highest value of R_s was for the DCMS device (9.47 Ω cm^2), and the lowest value of R_s was for the superimposed HiPIMS device (1.42 Ω cm^2). Further, we performed a four-point probe experiment to understand the electrical properties of Cu_2O. This analysis showed the highest value of electrical conductivity (σ) for the superimposed HiPIMS Cu_2O thin film (3.33 S cm^{-1}) and the lowest for the DCMS Cu_2O thin film (0.11 S cm^{-1}). In addition, through XRD analysis (Figure S2), the crystallinity of the Cu_2O improved from the DCMS to superimposed HiPIMS deposition techniques. According to previous studies, an increase in film's crystallinity helps to increase the charge-carrier mobility (μ) [50]. In addition, varying the exposure times of the sputtering and plasma treatments impacted the optoelectronic properties of the thin films. In an attempt to reduce the exposure time during sputtering, we observed that the quality of the Cu_2O film deteriorated significantly, potentially due to the film becoming discontinuous. Conversely, increasing the exposure time led to a well-formed Cu_2O film. However, it resulted in unsatisfactory formation of the perovskite layer, and we are currently investigating the underlying reasons for this. As for the plasma treatment, we have not yet examined the impact of different exposure times on the optoelectronic properties of Cu_2O film, as our primary goal was to improve its wettability. However, we speculate that excessively long exposure times during plasma treatment may damage Cu_2O film and decrease its photoelectric properties. Lower values of R_s appear to be associated with higher σ and μ of Cu_2O thin films and increased J_{sc} values of the device. We speculate that the increase in J_{sc} could have been due to a reduction in the carrier recombination

rate at the p-i interface. This explanation is supported by other studies reporting that increasing hole conductivity can lead to higher J_{sc} [51]. We acknowledge that we do not have the necessary facilities to perform spectral-response characterization experiments, but our findings align with the existing literature. Overall, the use of superimposed HiPIMS Cu_2O as HTLs resulted in higher FF, J_{sc}, and PCE values compared with the devices based on DCMS and HiPIMS. As indicated in Figure 4, 15.20% was the best performance of the superimposed HiPIMS devices. Table 2 compares Cu_2O films as the HTLs of PSCs prepared by different processes; V_{oc}, J_{sc}, FF, and PCE are the best performance values of the device. The Cu_2O films were prepared by various methods such as spin coating [52,53], successive ionic layer adsorption and reaction (SILAR) [54], sputtering [55,56], the thermal oxidation method [57,58], electrodeposition [59,60], chemical vapor deposition (CVD) [61], etc. Although it is known from simulation results that, theoretically, the PCE of Cu_2O-based PSCs can be as high as 25.2% [62], it was found that the actual device PCE was mostly in the range of 6 to 13%. Based on the above method, we observed that the improvement in PCE was due to the low series and high shunt resistance of the respective devices. The high conductivity of the Cu_2O thin film resulted in low recombination loss and smaller bulk resistance of the device. These factors contributed to a reduction in the energy loss within the device and increased the efficiency of charge extraction and transfer. This phenomenon is consistent with findings in previous reports [54,60].

Table 1. Different process technologies for solar cell devices.

Sample	J_{sc} (mA/cm^2)	V_{oc} (V)	FF (%)	PCE (%)	Best PCE (%)	R_s [a] (Ω cm^2)	R_{sh} [a] (Ω cm^2)	σ (S cm^{-1})
DCMS	13.74 ± 0.97	0.89 ± 0.02	58.1 ± 3.93	7.12 ± 0.64	7.91	9.47	111.82	0.11
HiPIMS	17.36 ± 0.94	0.90 ± 0.00	61.1 ± 6.95	9.42 ± 0.92	10.29	3.09	1081.18	0.40
Superimposed HiPIMS	19.27 ± 1.20	0.98 ± 0.00	69.5 ± 4.98	13.04 ± 1.61	15.20	1.42	1080.19	3.33

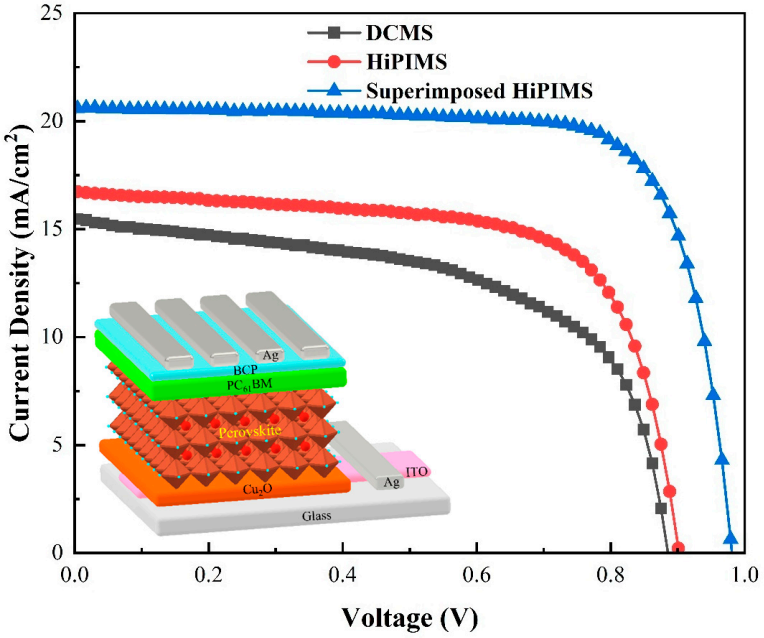

Figure 4. J–V curves of PSCs and device structure.

Table 2. Performances of Cu_2O HTLs in PSCs prepared by different process technologies in the literature.

Process Technology	J_{sc} (mA/cm^2)	V_{oc} (V)	FF (%)	PCE (%)	Year/Ref.
Spin Coating	16.52	1.07	75.5	13.35	2015/[52]
SILAR	16.52	0.89	56.0	8.23	2016/[54]
Rotating Sputtering	15.80	0.96	59.0	8.93	2016/[55]
Cu Thermal Oxidation	17.5	0.95	66.2	11.03	2016/[57]
Cu Thermal Oxidation	14.40	0.96	58.6	8.10	2016/[58]
Electrodeposition	18.03	0.88	61.0	9.64	2016/[59]
RF Sputtering	14.94	0.93	67.5	9.37	2018/[56]
CVD	17.50	0.98	48.0	8.26	2018/[61]
Electrodeposition	19.03	0.97	73.0	13.48	2019/[60]
Spin Coating	12.87	0.71	69.0	6.26	2021/[53]
Hydrothermal Technique	12.58	0.76	63.0	6.02	2022/[37]
Superimposed HiPIMS	20.34	0.98	76.5	15.20	This work

In this study, we achieved a competitive result of 15.21% via embedding Cu_2O thin films using superimposed HiPIMS. The MF power-supply sputtering in the superimposed HiPIMS system allowed us to retain a high ionization rate as the advantage of the HiPIMS. Compared with DCMS processes, HiPIMS and superimposed HiPIMS can bombard sputtering ions with higher energy, which helps to form the preferred stoichiometry of Cu_2O films, resulting in a denser coating with lower surface roughness. It helped to reduce the defects in the film and led to a smoother interface, resulting in a decrease in the leakage current and an improvement in the PCE. Our EPMA analysis (Table S1) showed that the Cu_2O chemical composition ratio as Cu/O was 1.9, which is close to the form of perfect stoichiometric Cu_2O.

In addition to evaluating the surface morphologies of the Cu_2O films, we also evaluated the energy level alignment at the Cu_2O/p-i interface using an incident light energy of 21.2 eV (He(I) emission) via ultraviolet photoelectron spectroscopy (UPS). Figure 5 presents the $E_{Cut\text{-}off}$ regions of the DCMS, HiPIMS, and superimposed HiPIMS Cu_2O samples ($WF = 21.2 - E_{Cut\text{-}off}$) [63,64]. The DCMS Cu_2O film had a work function (WF) of –6.40 eV, while the WF of the HiPIMS Cu_2O film was –6.38 eV, which was 0.02 eV lesser than that of the DCMS Cu_2O film. The WF of the superimposed HiPIMS sample was –6.07 eV (the negative work function means how much energy is required to be added to the bound electron by the photon it absorbs). Changes in the WF at the p-i interface can significantly impact the energy alignment of Cu_2O with perovskite, hole transport, and effectiveness of charge extraction as well as transfer. Therefore, a shift in the energy levels of the Cu_2O may have contributed to the improved performance of the Cu_2O devices. We believe that the significantly different composition ratio (Table S1) and phase structure (Figure S2) of the superimposed HiPIMS Cu_2O film may have affected the WF, resulting in the improved device performance.

We examined the shelf lives of the unencapsulated devices under an argon glove box in the dark to assess the stability of the superimposed HiPIMS Cu_2O sample for PSC applications (we measured the PCE results at least three times to calculate the error bars). The devices initially offered the best PCE of 15.20%, as shown in Figure 6. After testing for 168 h, the devices retained 99.4% of their initial performance; after testing over 1000 h, the devices retained 98.3% of their initial performance; and after testing over 2000 h, the devices retained 97.6% of their initial performance. Thus, our PSC device suggested high stability. Finally, we determined the performance of the superimposed HiPIMS device under dim light (a TL-84 fluorescent lamp with an illumination of 1000 lux). Table 3 shows the performance of the respective device. The device showed a PCE of 25.09%. Based on these results, we demonstrated that Cu_2O film has great potential as HTLs of PSCs under one sun and indoor illumination.

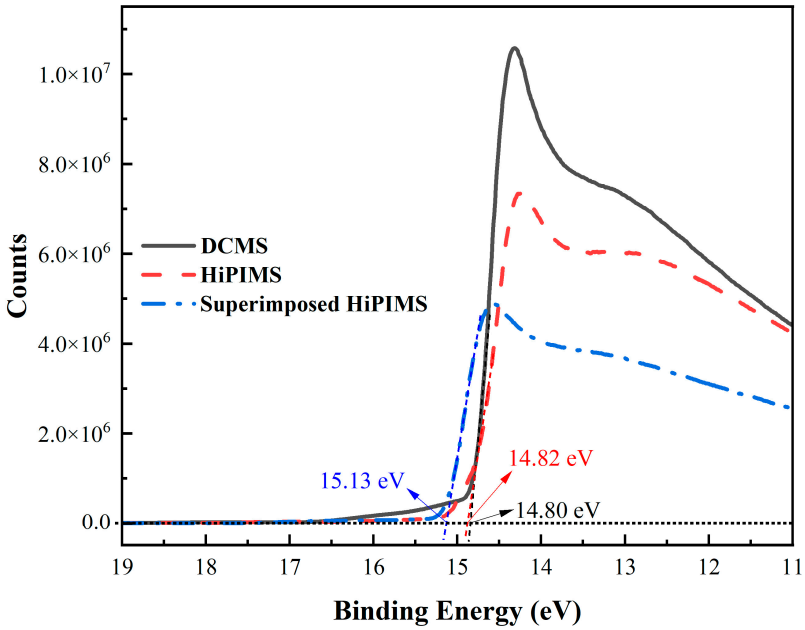

Figure 5. UPS spectra of ITO/Cu_2O films (DCMS, HiPIMS, and superimposed HiPIMS).

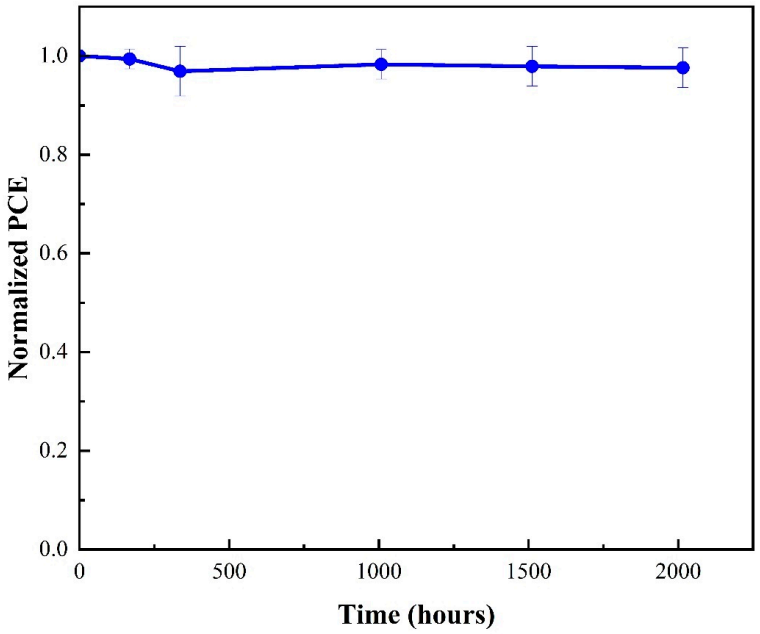

Figure 6. Stability data of unsealed devices from superimposed HiPIMS under the argon glove box.

Table 3. Superimposed HiPIMS device with dim light.

Sample	J_{sc} (μA/cm^2)	V_{oc} (V)	FF (%)	PCE (%)
Superimposed HiPIMS	189.51	0.62	66.4	25.09

4. Conclusions

In this study, we prepared Cu_2O films via DCMS, HiPIMS, and superimposed HiPIMS and used them as HTLs for PSC applications. In the comparison of different process technologies for Cu_2O samples, superimposed HiPIMS enhanced the WF (measured by UPS), surface roughness (measured by AFM), and optoelectronic properties of the Cu_2O films and, in turn, increased carrier extraction and transport at the perovskite–Cu_2O

interface. Because the optimized Cu_2O film was obtained from superimposed HiPIMS technology, we observed an increase in the PCE of the PSCs from 7.91 (DCMS) to 15.20%. The extended shelf life of the unencapsulated devices in the glove box attested to their excellent stability and support Cu_2O as a contender for p-type transporting layers in PSC applications.

Supplementary Materials: The following supporting information can be downloaded at: https://www.mdpi.com/article/10.3390/nano13081363/s1, Experimental Details, Figure S1: Cu_2O film prepared by (a) DCMS, (b) superimposed HiPIMS of contact angle.; Figure S2: X-ray diffraction spectra of different process technologies.; Table S1: Chemical composition of different process technologies. References [19,65,66] are cited in the supplementary materials.

Author Contributions: Conceptualization, T.-H.C. and S.-C.C.; data curation, Y.-H.C.; investigation, Y.-H.C.; writing—original draft preparation, S.S. and Y.-H.C.; writing—review and editing, S.S. and C.-P.C.; supervision, T.-H.C., W.-C.C., C.K.C., C.-P.C. and S.-C.C.; resources, T.-H.C. and S.-C.C. All authors have read and agreed to the published version of the manuscript.

Funding: We sincerely appreciate the financial assistance provided by the Ministry of Science and Technology of Taiwan (MOST 111-2221-E-131-027).

Acknowledgments: We thank H.-C. Lin and C.-Y. Kao of the Instrumentation Center, National Taiwan University for their assistance with the EPMA experiments.

Conflicts of Interest: The authors declare no conflict of interest.

References

1. Ellis, F., Jr.; Delahoy, A. Optical properties of hydrogenated amorphous silicon based solar cells. *Sol. Energy Mater.* **1986**, *13*, 109–132. [CrossRef]
2. Chen, S.; Kumar, R.V.; Gedanken, A.; Zaban, A. Sonochemical synthesis of crystalline nanoporous zinc oxide spheres and their application in dye-sensitized solar cells. *Isr. J. Chem.* **2001**, *41*, 51–54. [CrossRef]
3. Kushto, G.P.; Kim, W.; Kafafi, Z.H. Flexible organic photovoltaics using conducting polymer electrodes. *Appl. Phys. Lett.* **2005**, *86*, 093502. [CrossRef]
4. Jiang, B.H.; Peng, Y.J.; Su, Y.W.; Chang, J.F.; Chueh, C.C.; Shieh, T.S.; Huang, C.I.; Chen, C.P. A polymer donor with versatility for fabricating high-performance ternary organic photovoltaics. *Chem. Eng. J.* **2022**, *431*, 133950. [CrossRef]
5. Chen, W.; Wu, Y.; Yue, Y.; Liu, J.; Zhang, W.; Yang, X.; Chen, H.; Bi, E.; Ashraful, I.; Grätzel, M. Efficient and stable large-area perovskite solar cells with inorganic charge extraction layers. *Science* **2015**, *350*, 944–948. [CrossRef]
6. Lin, S.C.; Cheng, T.H.; Chen, C.P.; Chen, Y.C. Structural effect on triphenylamine dibenzofulvene based interfacial hole transporting materials for high-performance inverted perovskite solar cells. *Mater. Chem. Phys.* **2022**, *288*, 126385. [CrossRef]
7. Christians, J.A.; Schulz, P.; Tinkham, J.S.; Schloemer, T.H.; Harvey, S.P.; Tremolet de Villers, B.J.; Sellinger, A.; Berry, J.J.; Luther, J.M. Tailored interfaces of unencapsulated perovskite solar cells for >1000 hour operational stability. *Nat. Energy* **2018**, *3*, 68–74. [CrossRef]
8. Leijtens, T.; Giovenzana, T.; Habisreutinger, S.N.; Tinkham, J.S.; Noel, N.K.; Kamino, B.A.; Sadoughi, G.; Sellinger, A.; Snaith, H.J. Hydrophobic organic hole transporters for improved moisture resistance in metal halide perovskite solar cells. *ACS Appl. Mater. Interfaces* **2016**, *8*, 5981–5989. [CrossRef] [PubMed]
9. Mazzarella, L.; Lin, Y.H.; Kirner, S.; Morales Vilches, A.B.; Korte, L.; Albrecht, S.; Crossland, E.; Stannowski, B.; Case, C.; Snaith, H.J. Infrared light management using a nanocrystalline silicon oxide interlayer in monolithic perovskite/silicon heterojunction tandem solar cells with efficiency above 25%. *Adv. Energy Mater.* **2019**, *9*, 1803241. [CrossRef]
10. Jiang, Q.; Tong, J.; Xian, Y.; Kerner, R.A.; Dunfield, S.P.; Xiao, C.; Scheidt, R.A.; Kuciauskas, D.; Wang, X.; Hautzinger, M.P. Surface reaction for efficient and stable inverted perovskite solar cells. *Nature* **2022**, *611*, 278–283. [CrossRef]
11. Kojima, A.; Teshima, K.; Shirai, Y.; Miyasaka, T. Organometal halide perovskites as visible-light sensitizers for photovoltaic cells. *J. Am. Chem. Soc.* **2009**, *131*, 6050–6051. [CrossRef] [PubMed]
12. Kim, M.; Jeong, J.; Lu, H.; Lee, T.K.; Eickemeyer, F.T.; Liu, Y.; Choi, I.W.; Choi, S.J.; Jo, Y.; Kim, H.B. Conformal quantum dot–SnO_2 layers as electron transporters for efficient perovskite solar cells. *Science* **2022**, *375*, 302–306. [CrossRef] [PubMed]
13. Qin, P.L.; He, Q.; Chen, C.; Zheng, X.L.; Yang, G.; Tao, H.; Xiong, L.B.; Xiong, L.; Li, G.; Fang, G.J. High-Performance Rigid and Flexible Perovskite Solar Cells with Low-Temperature Solution-Processable Binary Metal Oxide Hole-Transporting Materials. *Sol. RRL* **2017**, *1*, 1700058. [CrossRef]
14. Qin, P.L.; Yang, G.; Ren, Z.W.; Cheung, S.H.; So, S.K.; Chen, L.; Hao, J.; Hou, J.; Li, G. Stable and efficient organo-metal halide hybrid perovskite solar cells via π-conjugated lewis base polymer induced trap passivation and charge extraction. *Adv. Mater.* **2018**, *30*, 1706126. [CrossRef] [PubMed]

15. Zhu, H.L.; Liang, Z.; Huo, Z.; Ng, W.K.; Mao, J.; Wong, K.S.; Yin, W.J.; Choy, W.C. Low-Bandgap Methylammonium-Rubidium Cation Sn-Rich Perovskites for Efficient Ultraviolet–Visible–Near Infrared Photodetectors. *Adv. Funct. Mater.* **2018**, *28*, 1706068. [CrossRef]
16. Zhu, Z.; Zhao, D.; Chueh, C.C.; Shi, X.; Li, Z.; Jen, A.K.Y. Highly efficient and stable perovskite solar cells enabled by all-crosslinked charge-transporting layers. *Joule* **2018**, *2*, 168–183. [CrossRef]
17. Correa Baena, J.P.; Saliba, M.; Buonassisi, T.; Grätzel, M.; Abate, A.; Tress, W.; Hagfeldt, A. Promises and challenges of perovskite solar cells. *Science* **2017**, *358*, 739–744. [CrossRef]
18. Huang, J.; Yuan, Y.; Shao, Y.; Yan, Y. Understanding the physical properties of hybrid perovskites for photovoltaic applications. *Nat. Rev. Mater.* **2017**, *2*, 17042. [CrossRef]
19. Hsu, H.L.; Hsiao, H.T.; Juang, T.Y.; Jiang, B.H.; Chen, S.C.; Jeng, R.J.; Chen, C.P. Carbon nanodot additives realize high-performance air-stable p–i–n perovskite solar cells providing efficiencies of up to 20.2%. *Adv. Energy Mater.* **2018**, *8*, 1802323. [CrossRef]
20. Singh, M.; Ng, A.; Ren, Z.; Hu, H.; Lin, H.C.; Chu, C.W.; Li, G. Facile synthesis of composite tin oxide nanostructures for high-performance planar perovskite solar cells. *Nano Energy* **2019**, *60*, 275–284. [CrossRef]
21. Zhang, H.; Nazeeruddin, M.K.; Choy, W.C. Perovskite photovoltaics: The significant role of ligands in film formation, passivation, and stability. *Adv. Mater.* **2019**, *31*, 1805702. [CrossRef] [PubMed]
22. Ono, L.K.; Juarez Perez, E.J.; Qi, Y. Progress on perovskite materials and solar cells with mixed cations and halide anions. *ACS Appl. Mater. Interfaces* **2017**, *9*, 30197–30246. [CrossRef] [PubMed]
23. Lee, K.M.; Chen, K.S.; Wu, J.R.; Lin, Y.D.; Yu, S.M.; Chang, S.H. Highly efficient and stable semi-transparent perovskite solar modules with a trilayer anode electrode. *Nanoscale* **2018**, *10*, 17699–17704. [CrossRef] [PubMed]
24. Hsu, H.L.; Chen, C.P.; Chang, J.Y.; Yu, Y.Y.; Shen, Y.K. Two-step thermal annealing improves the morphology of spin-coated films for highly efficient perovskite hybrid photovoltaics. *Nanoscale* **2014**, *6*, 10281–10288. [CrossRef]
25. Zeng, X.; Zhou, T.; Leng, C.; Zang, Z.; Wang, M.; Hu, W.; Tang, X.; Lu, S.; Fang, L.; Zhou, M. Performance improvement of perovskite solar cells by employing a CdSe quantum dot/PCBM composite as an electron transport layer. *J. Mater. Chem. A* **2017**, *5*, 17499–17505. [CrossRef]
26. Cao, X.; Zhi, L.; Jia, Y.; Li, Y.; Zhao, K.; Cui, X.; Ci, L.; Zhuang, D.; Wei, J. A review of the role of solvents in formation of high-quality solution-processed perovskite films. *ACS Appl. Mater. Interfaces* **2019**, *11*, 7639–7654. [CrossRef]
27. Li, S.; Ren, H.; Yan, Y. Boosting efficiency of planar heterojunction perovskite solar cells to 21.2% by a facile two-step deposition strategy. *Appl. Surf. Sci.* **2019**, *484*, 1191–1197. [CrossRef]
28. Lin, Z.; Li, J.; Li, H.; Mo, Y.; Pan, J.; Wang, C.; Zhang, X.L.; Bu, T.; Zhong, J.; Cheng, Y.B. A novel dopant for spiro-OMeTAD towards efficient and stable perovskite solar cells. *Sci. China Mater.* **2021**, *64*, 2915–2925. [CrossRef]
29. Li, P.; Mohamed, M.I.O.; Xu, C.; Wang, X.; Tang, X. Electrical property modified hole transport layer (PEDOT: PSS) enhance the efficiency of perovskite solar cells: Hybrid co-solvent post-treatment. *Org. Electron.* **2020**, *78*, 105582. [CrossRef]
30. Zhang, Y.; Liu, W.; Tan, F.; Gu, Y. The essential role of the poly (3-hexylthiophene) hole transport layer in perovskite solar cells. *J. Power Sources* **2015**, *274*, 1224–1230. [CrossRef]
31. Wang, Y.; Duan, L.; Zhang, M.; Hameiri, Z.; Liu, X.; Bai, Y.; Hao, X. PTAA as Efficient Hole Transport Materials in Perovskite Solar Cells: A Review. *Sol. RRL* **2022**, *6*, 2200234. [CrossRef]
32. Lin, Y.R.; Liao, Y.S.; Hsiao, H.T.; Chen, C.P. Two-step annealing of NiO_x enhances the NiO_x–perovskite interface for high-performance ambient-stable p–i–n perovskite solar cells. *Appl. Surf. Sci.* **2020**, *504*, 144478. [CrossRef]
33. Cao, J.; Yu, H.; Zhou, S.; Qin, M.; Lau, T.K.; Lu, X.; Zhao, N.; Wong, C.P. Low-temperature solution-processed NiO_x films for air-stable perovskite solar cells. *J. Mater. Chem. A* **2017**, *5*, 11071–11077. [CrossRef]
34. Musa, A.; Akomolafe, T.; Carter, M. Production of cuprous oxide, a solar cell material, by thermal oxidation and a study of its physical and electrical properties. *Sol. Energy Mater. Sol. Cells* **1998**, *51*, 305–316. [CrossRef]
35. Abdelfatah, M.; Ledig, J.; El-Shaer, A.; Wagner, A.; Sharafeev, A.; Lemmens, P.; Mosaad, M.M.; Waag, A.; Bakin, A. Fabrication and characterization of flexible solar cell from electrodeposited Cu_2O thin film on plastic substrate. *Sol. Energy* **2015**, *122*, 1193–1198. [CrossRef]
36. Rühle, S.; Barad, H.; Bouhadana, Y.; Keller, D.; Ginsburg, A.; Shimanovich, K.; Majhi, K.; Lovrincic, R.; Anderson, A.; Zaban, A. Combinatorial solar cell libraries for the investigation of different metal back contacts for TiO_2–Cu_2O hetero-junction solar cells. *Phys. Chem. Chem. Phys.* **2014**, *16*, 352156. [CrossRef]
37. Aseena, S.; Abraham, N.; Sahaya Dennish Babu, G.; Kathiresan, S.; Suresh Babu, V. Solution-Synthesized Cu_2O as a Hole Transport Layer for a ZnO-Based Planar Heterojunction Perovskite Solar Cell Fabricated at Room Temperature. *J. Electron. Mater.* **2022**, *51*, 1692–1699. [CrossRef]
38. Jeong, S.; Mittiga, A.; Salza, E.; Masci, A.; Passerini, S. Electrodeposited ZnO/Cu_2O heterojunction solar cells. *Electrochim. Acta* **2008**, *53*, 2226–2231. [CrossRef]
39. Yu, L.; Xiong, L.; Yu, Y. Cu_2O homojunction solar cells: F-doped N-type thin film and highly improved efficiency. *J. Phys. Chem. C* **2015**, *119*, 22803–22811. [CrossRef]
40. Halin, D.; Talib, I.; Daud, A.; Hamid, M. Characterizations of cuprous oxide thin films prepared by sol-gel spin coating technique with different additives for the photoelectrochemical solar cell. *Int. J. Photoenergy* **2014**, *2014*, 352156. [CrossRef]

41. Chua, D.; Kim, S.B.; Gordon, R. Enhancement of the open circuit voltage of Cu_2O/Ga_2O_3 heterojunction solar cells through the mitigation of interfacial recombination. *AIP Adv.* **2019**, *9*, 055203. [CrossRef]
42. Sanjana, T.; Sunil, M.A.; Shaik, H.; Kumar, K.N. Studies on DC sputtered cuprous oxide thin films for solar cell absorber layers. *Mater. Chem. Phys.* **2022**, *281*, 125922. [CrossRef]
43. Yang, F.F.; Peng, W.B.; Zhou, Y.J.; Li, R.; Xiang, G.J.; Yue Liu, J.M.Z.; Zhang, J.H.; Zhao, Y.; Wang, H. Thermal optimization of defected Cu_2O photon-absorbing layer and the steady p-Cu_2O/n-Si photovoltaic application. *Vacuum* **2022**, *198*, 110876. [CrossRef]
44. Georgieva, V.; Ristov, M. Electrodeposited cuprous oxide on indium tin oxide for solar applications. *Sol. Energy Mater. Sol. Cells* **2002**, *73*, 67–73. [CrossRef]
45. Kartha, C.V.; Rehspringer, J.L.; Muller, D.; Roques, S.; Bartringer, J.; Ferblantier, G.; Slaoui, A.; Fix, T. Insights into Cu_2O thin film absorber via pulsed laser deposition. *Ceram. Int.* **2022**, *48*, 15274–15281. [CrossRef]
46. Sun, H.; Chen, S.C.; Wen, C.K.; Chuang, T.H.; Yazdi, M.A.P.; Sanchette, F.; Billard, A. p-type cuprous oxide thin films with high conductivity deposited by high power impulse magnetron sputtering. *Ceram. Int.* **2017**, *43*, 6214–6220. [CrossRef]
47. Sun, H.; Kuo, T.Y.; Chen, S.C.; Chen, Y.H.; Lin, H.C.; Yazdi, M.A.P.; Billard, A. Contribution of enhanced ionization to the optoelectronic properties of p-type NiO films deposited by high power impulse magnetron sputtering. *J. Eur. Ceram. Soc.* **2019**, *39*, 5285–5291. [CrossRef]
48. Chuang, T.H.; Wen, C.K.; Chen, S.C.; Liao, M.H.; Liu, F.; Sun, H. p-type semi-transparent conductive NiO films with high deposition rate produced by superimposed high power impulse magnetron sputtering. *Ceram. Int.* **2020**, *46*, 27695–27701. [CrossRef]
49. Sun, H.; Wen, C.K.; Chen, S.C.; Chuang, T.H.; Arab Pour Yazdi, M.; Sanchette, F.; Billard, A. Microstructures and optoelectronic properties of Cu_xO films deposited by high-power impulse magnetron sputtering. *J. Alloys Compd.* **2016**, *688*, 672–678. [CrossRef]
50. Sakalley, S.; Saravanan, A.; Cheng, W.C.; Chen, S.C.; Sun, H.; Liao, M.H.; Huang, B.R. Cu_3N thin film synthesized by selective in situ substrate heating during high power impulse magnetron sputtering for augmenting UV photodetection. *Sens. Actuator A Phys.* **2023**, *350*, 114137. [CrossRef]
51. Yao, Q.; Zhao, L.; Sun, X.; Zhu, L.; Zhao, Y.; Qiang, Y.; Song, J. Na_2S decorated NiO_x as effective hole transport layer for inverted planar perovskite solar cells. *Mater. Sci. Semicond. Process.* **2023**, *153*, 107107. [CrossRef]
52. Zuo, C.; Ding, L. Solution-Processed Cu_2O and CuO as Hole Transport Materials for Efficient Perovskite Solar Cells. *Small* **2015**, *11*, 5528–5532. [CrossRef] [PubMed]
53. Makenali, M.; Kazeminezhad, I.; Ahmadi, V.; Roghabadi, F.A. Charge transfer balancing of planar perovskite solar cell based on a low cost and facile solution-processed CuO_x as an efficient hole transporting layer. *J. Mater. Sci. Mater. Electron.* **2021**, *32*, 2312–2325. [CrossRef]
54. Chatterjee, S.; Pal, A.J. Introducing Cu_2O Thin Films as a Hole-Transport Layer in Efficient Planar Perovskite Solar Cell Structures. *J. Phys. Chem. C* **2016**, *120*, 1428–1437. [CrossRef]
55. Nejand, B.A.; Ahmadi, V.; Gharibzadeh, S.; Shahverdi, H.R. Cuprous Oxide as a Potential Low-Cost Hole-Transport Material for Stable Perovskite Solar Cells. *ChemSusChem* **2016**, *9*, 302–313. [CrossRef]
56. Chen, Y.J.; Li, M.H.; Huang, J.C.A.; Chen, P. The Cu/Cu_2O nanocomposite as a p-type transparent-conductive-oxide for efficient bifacial-illuminated perovskite solar cells. *J. Mater. Chem. C* **2018**, *6*, 6280–6286. [CrossRef]
57. Yu, W.; Li, F.; Wang, H.; Alarousu, E.; Chen, Y.; Lin, B.; Wang, L.; Hedhili, M.N.; Li, Y.; Wu, K.; et al. Ultrathin Cu_2O as an efficient inorganic hole transporting material for perovskite solar cells. *Nanoscale* **2016**, *8*, 6173–6179. [CrossRef]
58. Chen, L.C.; Chen, C.C.; Liang, K.C.; Chang, S.H.; Tseng, Z.L.; Yeh, S.C.; Chen, C.T.; Wu, W.T.; Wu, C.G. Nano-structured CuO-Cu_2O Complex Thin Film for Application in $CH_3NH_3PbI_3$ Perovskite Solar Cells. *Nanoscale Res. Lett.* **2016**, *11*, 402. [CrossRef]
59. Liu, L.; Xi, Q.; Gao, G.; Yang, W.; Zhou, H.; Zhao, Y.; Wu, C.; Wang, L.; Xu, J. Cu_2O particles mediated growth of perovskite for high efficient hole-transporting-layer free solar cells in ambient conditions. *Sol. Energy Mater. Sol. Cells* **2016**, *157*, 937–942. [CrossRef]
60. Miao, X.; Wang, S.; Sun, W.; Zhu, Y.; Du, C.; Ma, R.; Wang, C. Effect of Cu_2O Content in Electrodeposited CuO_x Film on Perovskite Solar Cells. *Nano* **2019**, *14*, 1950126. [CrossRef]
61. Zhang, Z.; Chen, S.; Li, P.; Li, H.; Wu, J.; Hu, P.; Wang, J. Aerosol-assisted chemical vapor deposition of ultra-thin CuO_x films as hole transport material for planar perovskite solar cells. *Funct. Mater. Lett.* **2018**, *11*, 1850035. [CrossRef]
62. Sajid, S.; Alzahmi, S.; Salem, I.B.; Obaidat, I.M. Guidelines for Fabricating Highly Efficient Perovskite Solar Cells with Cu_2O as the Hole Transport Material. *Nanomaterials* **2022**, *12*, 3315. [CrossRef] [PubMed]
63. Ravindra, P.; Mukherjee, R.; Avasthi, S. Hole-selective electron-blocking copper oxide contact for silicon solar cells. *IEEE J. Photovolt.* **2017**, *7*, 1278–1283. [CrossRef]
64. Guo, Y.; Lei, H.; Xiong, L.; Li, B.; Chen, Z.; Wen, J.; Yang, G.; Li, G.; Fang, G. Single phase, high hole mobility Cu_2O films as an efficient and robust hole transporting layer for organic solar cells. *J. Mater. Chem. A* **2017**, *5*, 11055–11062. [CrossRef]

65. Lee, J.W.; Bae, S.H.; Hsieh, Y.T.; De Marco, N.; Wang, M.; Sun, P.; Yang, Y. A bifunctional lewis base additive for microscopic homogeneity in perovskite solar cells. *Chem.* **2017**, *3*, 290–302. [CrossRef]
66. Hsieh, C.M.; Liao, Y.S.; Lin, Y.R.; Chen, C.P.; Tsai, C.M.; Diau, E.W.G.; Chuang, S.C. Low-temperature, simple and efficient preparation of perovskite solar cells using Lewis bases urea and thiourea as additives: Stimulating large grain growth and providing a PCE up to 18.8%. *RSC Adv.* **2018**, *8*, 19610–19615. [CrossRef]

Disclaimer/Publisher's Note: The statements, opinions and data contained in all publications are solely those of the individual author(s) and contributor(s) and not of MDPI and/or the editor(s). MDPI and/or the editor(s) disclaim responsibility for any injury to people or property resulting from any ideas, methods, instructions or products referred to in the content.